Manuscript submitted to the 9th Holistic Innovation in Additive Manufacturing Conference (HI-AM 2026).
This preprint has not been peer-reviewed and is not an official HI-AM Conference publication.

Application of process-integrated laser treatment for microstructure-induced distortion control in PBF-LB/M

Jork Groenewold[1,*], Stefan Seifert[1], Martin Benfer[1], Gisela Lanza[1]

[1] wbk Institute of Production Science, Karlsruhe Institute of Technology (KIT), Kaiserstr. 12, 76131 Karlsruhe, Germany

* Corresponding author's email address: jork.groenewold@kit.edu

Abstract: Additive manufacturing of metal components by powder bed fusion using a laser beam (PBF-LB/M) is widely used for producing complex geometries. However, process-induced residual stresses, which can lead to distortion and cracking, thereby limiting geometric accuracy, remain a challenge. This work presents an integrated process-level approach to mitigate these effects by locally influencing the microstructure during fabrication through targeted laser-based treatment to reduce residual stresses. The approach is investigated experimentally using cantilever geometries, which serve as a benchmark for quantifying distortion caused by residual stresses. Based on the observed deformation behavior, the effectiveness of the proposed strategy in reducing process-induced distortion is assessed. The insights gained with these simple test geometries are subsequently applied to a real industrial component to evaluate the approach's broader applicability. A reduction in geometric deviation is observed when applying the proposed strategy, indicating its potential to mitigate distortion in practical PBF-LB/M applications. Overall, the study demonstrates that process-integrated laser treatment can influence the development of residual stress and associated distortion during PBF-LB/M. This helps enable broader, more reliable use of metal additive manufacturing in industrial applications.

Keywords: Additive manufacturing, Powder bed fusion of metals using a laser beam (PBF-LB/M), Residual stress, Microstructure, Process-integrated laser treatment.

---

1. Introduction

Powder bed fusion of metal by laser beam (PBF-LB/M) enables the layer-wise fabrication of geometrically complex parts, but the localized melting and rapid solidification inherent to the process generate residual stresses that drive part distortion and cracking [1,2]. They are particularly pronounced in tool steels such as H13, whose martensitic transformation couples phase composition directly to the local stress state [3,4]. Established mitigation strategies such as preheating, scan-strategy optimisation and post-process annealing [1,5] act globally and rarely eliminate residual stresses entirely. A more selective alternative is to influence the microstructure layer by layer during fabrication. Selective laser treatment (LT) of solidified layers shifts the retained austenite content, thereby altering the local volumetric change, which in turn modulates the residual stress state. Realizing such control in practice requires (i) an on-machine measurement of the current microstructural state of each layer, and (ii) a process model that maps laser-treatment parameters to the resulting microstructure. Previous work by the authors demonstrated that eddy current (EC) sensing integrated into the recoater of an industrial PBF-LB/M system can detect LT-induced microstructural changes on H13 [6], and that Bayesian optimization (BO) with a Gaussian process (GP) surrogate efficiently learns the parameter-to-microstructure mapping [7]. The present work closes the remaining gap by demonstrating that the BO-identified parameter sets actually reduce the process-induced distortion when applied during PBF-LB/M. Effectiveness is first quantified on cantilever benchmarks and then transferred to an industrial heat-exchanger component manufactured under production conditions.

2. Materials and methods

2.1. Material and PBF-LB/M process

Experiments were performed on an SLM 280 HL machine (Nikon SLM Solutions). The material was AISI H13 tool steel, selected for its pronounced martensitic transformation [3,4]. The build parameters were held constant throughout all experiments and follow a previously optimized set: layer thickness 30 micrometers, laser power 250 W, scan speed 750 mm/s, hatch distance 0.09 mm, focus offset -4 mm and build-plate preheating temperature of 200 °C.

2.2. Laser treatment (LT) approach

Selective LT is applied between recoating steps using the same laser as the build exposure, so no additional hardware is required, and locally shifts the retained austenite content (V_γ) and the associated volumetric contribution to the residual stress state. Two contrasting parameter sets were extracted as the extrema of the GP surrogate model from earlier work [7]: parameter set L for minimum V_γ and parameter set H for maximum V_γ (Table 1). Set L (high scan speed v_s and large hatch distance d_h) produces a low areal energy density of $E_A = 1.28$ J/mm² and high cooling rates that favor martensite formation. Set H (low v_s, small d_h) yields 45.05 J/mm² and slower cooling that retains austenite.

Table 1: Optimized laser treatment (LT) parameter sets L and H identified by Bayesian optimization.

Set	P_L **[W]**	v_s**[mm/s]**	f_f **[mm]**	d_h **[mm]**	E_A **[J/mm²]**	V_γ **[%]**
H (max. V_γ)	92.73	205.82	-4.45	0.010	45.05	25.2
L (min. V_γ)	76.78	300.00	0.00	0.200	1.28	14.7

2.3. Cantilever benchmark geometry

Cantilever benchmarks quantify PBF-LB/M residual stresses: after separation from the build plate, stress relaxation manifests as an end deflection that serves as a geometry-amplified distortion metric [8, 9]. Specimens of 70 mm x 12 mm x 6.45 mm were fabricated and selectively laser-treated on the upper surface with a 4 mm x 4 mm checkerboard pattern (Figure 1) using parameter sets L and H. An unprocessed reference (REF) was included.

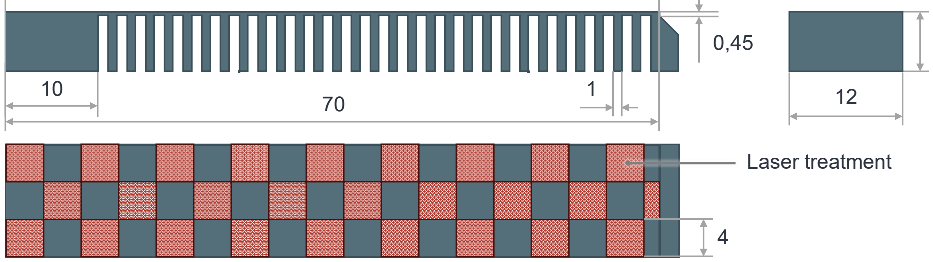

Figure 1: Cantilever geometry and treatment pattern checkerboard (4 mm x 4 mm fields).

After laser treatment, the support structures were severed by wire-EDM and the resulting deflection profile was recorded by a *Mahr MarSurf XCR 20* perthometer, with the maximum deflection at the free end (d_z) as distortion metric. Surface residual stresses (σ_{ES}) and V_γ were measured by XRD on a *Stresstech XStress DR45* (Cr-K-alpha, 30 kV, 9 mA, 1 mm collimator), using the modified χ method for stress and ASTM E975 for V_γ [10]. Six measurement positions per specimen were used. The checkerboard layout allows stress measurement separately in treated and adjacent untreated fields.

2.4. Industrial component transfer

To assess practical applicability, the LT strategy was transferred to a heat exchanger geometry from Fraunhofer IWU. Overhang regions, which are particularly prone to dimensional deviation in the absence of support structures, were targeted by scheduling LT in a 1 mm-thick band directly above each overhang after the corresponding build layer. One half of the heat exchanger was manufactured with this strategy and the other half conventionally without LT, enabling a direct intra-part comparison by X-ray computed tomography (CT) against the CAD reference.

3. Results and discussion

3.1. Cantilever benchmark results

Table 2 summarizes the residual stress, retained austenite, and distortion measurements for the three cantilever conditions. Figure 2 shows the corresponding perthometer deflection profiles.

Table 2: V_γ and surface residual stress σ_{ES} and maximum deflection z_A for the three cantilever conditions.

Condition	V_γ **treated [%]**	V_γ **untreated [%]**	σ_{ES} **treated [MPa]**	σ_{ES} **untreated [MPa]**	d_z **[mm]**
REF		9.7 ± 1.3		-284.3 ± 23.8	-2.60 ± 0.06
SBM-L	7.5 ± 0.9	8.8 ± 1.4	+76.5 ± 9.4	-231.2 ± 28.5	+0.10 ± 0.03
SBM-H	9.2 ± 3.1	8.6 ± 1.6	-482.4 ± 52.8	-331.4 ± 31.3	-1.12 ± 0.06

The XRD measurements show that the V_γ contrast is only partially reproduced on the checkerboard cantilever specimens. The retained austenite content in the treated fields was 7.5 ± 0.9 % for SBM-L and 9.2 ± 3.1 % for SBM-H, with the adjacent untreated fields at 8.8 ± 1.4 % (SBM-L) and 8.6 ± 1.6 % (SBM-H), respectively. The attenuated in-field contrast is consistent with lateral heat conduction across the 4 mm fields and indicates that the L/H stress contrast is driven by treatment depth and cooling rate rather than by the retained-austenite endpoint alone.

The surface residual stresses on the treated fields show that LB controls the stress state in both magnitude and sign. The reference state is in compression at σ_{ES} = -284.3 ± 23.8 MPa, in agreement with literature reports for as-built PBF-LB/M H13 [4,11]. Parameter set L produces a tensile state of σ_{ES} = +76.5 ± 9.4 MPa in the treated fields, while parameter set H further intensifies the compressive state to σ_{ES} = -482.4 ± 52.8 MPa.

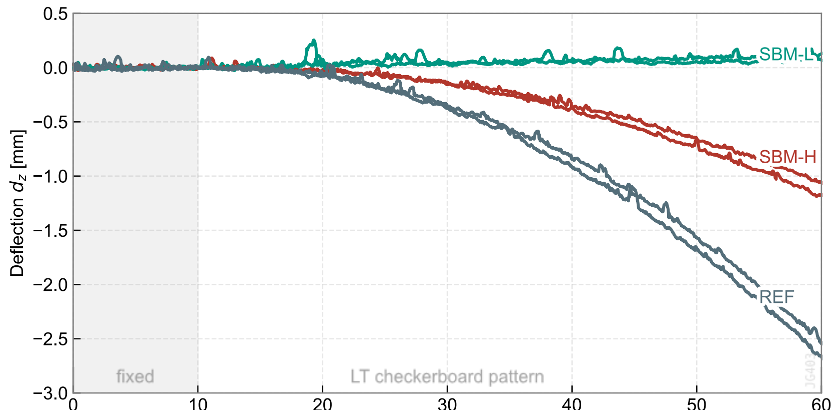

Figure 2: Perthometer deflection for the checkerboard cantilevers.

The observed stress polarity could be explained by interplay of two competing mechanisms: thermal contraction during the LB cooling cycle, which generates tensile stress, and the volumetric expansion of about 1 % accompanying the martensitic transformation [12], which generates a compressive contribution in the transformed zone. For parameter set L, the low energy density (1.28 J/mm²) confines austenitization to a shallow layer; the transformation expansion is insufficient to overcome the thermal tension, and a tensile net state remains. For parameter set H, the higher energy density (45.05 J/mm²) drives deeper austenitization, and the larger transformed volume, driven by depth rather than transformed fraction, overcompensates the thermal tension, yielding a strong compressive state. This interpretation is consistent with previous studies on laser surface treatment of H13 and AM steels [13,14]. The perthometer measurements confirm that these stress-state changes translate into a measurable reduction of part distortion. For reference, the maximum deflection at the free end is $d_{z,REF}$ = -2.60 ± 0.06 mm. Parameter set H reduces this to -1.12 ± 0.06 mm, a 57 % reduction relative to REF. Parameter set L over-compensates the residual-stress-induced bending entirely (d_z= +0.10 ± 0.03 mm).

3.2. Industrial component results

The CT-based comparison shows a small but consistent improvement in the treated half. The area fraction within ±0.05 mm of the CAD geometry increases from 35.66 % to 37.22 %, the fraction with deviation below −0.05 mm (sinking) decreases from 38.76 % to 37.69 %, and the fraction above +0.05 mm (over-building) decreases from 25.59 % to 25.09%. The improvement acts on both deviation tails, indicating both a distribution shift and an reduction of geometric error.

The smaller improvement than on the cantilever reflects the heat exchanger's stiffer 3-D topology, in which residual stresses partly self-equilibrate, and the deliberately selective LT scope of 1-mm bands above overhangs only (see Figure 3). The consistent improvement across all three deviation bands nonetheless shows that the strategy transfers from benchmark to production geometry without introducing new defects.

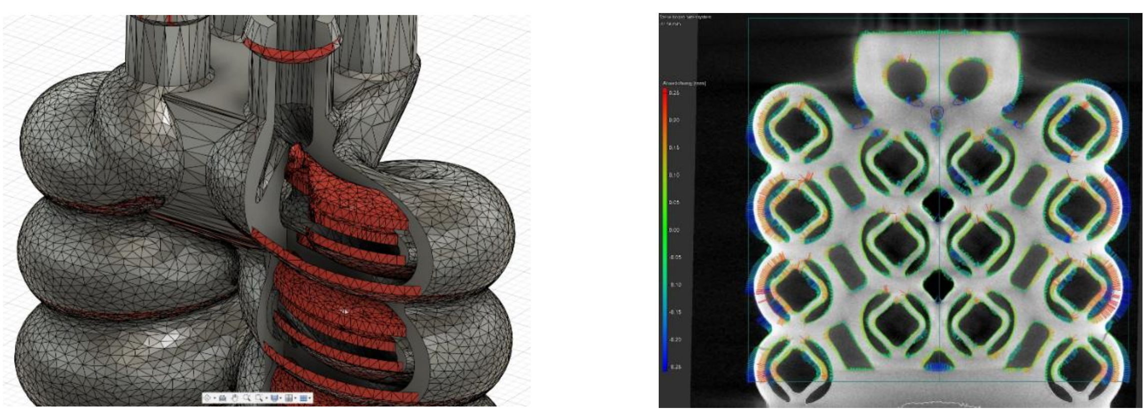
Figure 3: CAD model of the heat exchanger with marked LT regions (left) and CT-based actual-vs.-target deviation analysis of as-built part (right).

The process-time overhead was estimated for a generic 10 mm reference cube of 333 layers and 100 mm² per layer, which yields a baseline exposure time of about 8.2 min at the build parameters used here. Applying parameter set H to ten critical layers adds 1.7 % (+0.14 min) on top of the build, and full coverage of all layers with set H adds 56 %. Set L, with its smaller hatch distance, multiplies the build time when applied across all layers and is therefore restricted to localised hotspots. The selective application of set H thus stays in a range that is industrially acceptable for the demonstrated distortion reduction.

4. Conclusion

This work demonstrates that process-integrated laser heat treatment control the microstructure of PBF-LB/M H13 tool steel, translating into a measurable reduction of process-induced distortion. Using BO-derived parameter sets, surface residual stresses ranging from +76.5 MPa to -482.4 MPa were established. The corresponding cantilever deflection was reduced by 57 % for parameter set H and fully compensated, with slight overshoot, for parameter set L. The transfer to an industrial heat exchanger produced a small but consistent improvement of the dimensional-accuracy distribution at an industrially acceptable process-time overhead, confirming applicability beyond benchmark geometries.

Beyond retained austenite alone, the stress state is governed by transformation depth and cooling-rate-driven kinetics; the laser treatment also affects transformation depth, hardness gradients and possibly anisotropy. These were not characterised here and must be quantified before the approach is used on safety- or fatigue-critical components. Two steps remain for production use: the stacking of LT over consecutive layers requires systematic study, since successive thermal histories modify microstructure development; and the EC-based condition and GP-based process models must be coupled in a closed loop that adjusts each layer's LT parameters in-process. A direct on-machine residual-stress measurement, currently the open item in the sensing stack, would eventually let the loop close on the actual control target rather than its microstructural surrogate.

Acknowledgments

This research and development project is funded by the German Federal Ministry of Research, Technology and Space (BMFTR) within the “Future of Value Creation – Research on Production, Services and Work” program (funding number 02J23C100) and managed by the Project Management Agency Karlsruhe (PTKA), and within the “Additive Fertigung von hocheffizienten Wärmetauschern für Wasserstoff-Elektrolyseure” project (funding number 03SF0760A). The authors thank the Fraunhofer Institute for Nondestructive Testing (IZFP) for their scientific collaboration, and the Fraunhofer Institute for Machine Tools and Forming Technology (IWU) for providing the geometry of the industrial component.

References

[1] Bernard A, Kruth J-P, Cao J, Lanza G, Bruschi S, Merklein M, et al. Vision on metal additive manufacturing: Developments, challenges and future trends. CIRP Journal of Manufacturing Science and Technology 2023;47:18–58. https://doi.org/10.1016/j.cirpj.2023.08.005.

[2] Gibson I, Rosen D, Stucker B, Khorasani M. Additive manufacturing technologies. 3rd edition. Cham: Springer; 2021.

[3] Yan JJ, Zheng DL, Li HX, Jia X, Sun JF, Li YL, et al. Selective laser melting of H13: microstructure and residual stress. J Mater Sci 2017;52:12476–85. https://doi.org/10.1007/s10853-017-1380-3.

[4] Narvan M, Ghasemi A, Fereiduni E, Kendrish S, Elbestawi M. Part deflection and residual stresses in laser powder bed fusion of H13 tool steel. Materials & Design 2021;204:109659. https://doi.org/10.1016/j.matdes.2021.109659.

[5] Kaess M, Werz M, Weihe S. Residual Stress Formation Mechanisms in Laser Powder Bed Fusion—A Numerical Evaluation. Materials 2023;16:2321. https://doi.org/10.3390/ma16062321.

[6] Groenewold J, Hammes J, Stamer F, Lanza G. Influencing Residual Stress in PBF-LB/M Processes through In-Process Microstructure Assessment and Selective Laser Heat Treatment. In: Beaman JJ, Kovar D, Cullinan M, Sha Z, Crawford R, Tilton M, editors. Proceedings of the 35th annual international SOLID FREEFORM FABRICATION SYMPOSIUM 2024, 2024, p. 1027–35. https://doi.org/10.26153/tsw/58156.

[7] Groenewold J, Mai D, Stamer F, Lanza G. Modeling Process–Microstructure Relations in PBF-LB/M Laser Treatment using Gaussian Process Surrogates and Bayesian Optimization. Karlsruher Institut für Technologie (KIT); 2026. https://doi.org/10.5445/IR/1000189041.

[8] Kruth J-P, Deckers J, Yasa E, Wauthlé R. Assessing and comparing influencing factors of residual stresses in selective laser melting using a novel analysis method. Proceedings of the Institution of Mechanical Engineers, Part B: Journal of Engineering Manufacture 2012;226:980–91. https://doi.org/10.1177/0954405412437085.

[9] Robinson J, Ashton I, Fox P, Jones E, Sutcliffe C. Determination of the effect of scan strategy on residual stress in laser powder bed fusion additive manufacturing. Additive Manufacturing 2018;23:13–24. https://doi.org/10.1016/j.addma.2018.07.001.

[10] Advance Standards Transforming Markets (ASTM). Practice for X-Ray Determination of Retained Austenite in Steel with Near Random Crystallographic Orientation 2022. https://doi.org/10.1520/E0975-22.

[11] Mertens R, Vrancken B, Holmstock N, Kinds Y, Kruth J-P, Van Humbeeck J. Influence of Powder Bed Preheating on Microstructure and Mechanical Properties of H13 Tool Steel SLM Parts. Physics Procedia 2016;83:882–90. https://doi.org/10.1016/j.phpro.2016.08.092.

[12] Roos E, Maile K, Seidenfuß M. Werkstoffkunde für Ingenieure: Grundlagen, Anwendung, Prüfung. Berlin, Heidelberg: Springer Berlin Heidelberg; 2017. https://doi.org/10.1007/978-3-662-49532-2.

[13] Telasang G, Dutta Majumdar J, Padmanabham G, Manna I. Structure–property correlation in laser surface treated AISI H13 tool steel for improved mechanical properties. Materials Science and Engineering: A 2014;599:255–67. https://doi.org/10.1016/j.msea.2014.01.083.

[14] Zhang J, Yu M, Li Z, Liu Y, Zhang Q, Jiang R, et al. The effect of laser energy density on the microstructure, residual stress and phase composition of H13 steel treated by laser surface melting. Journal of Alloys and Compounds 2021;856:158168. https://doi.org/10.1016/j.jallcom.2020.158168.